Journal of the Korean Physical Society, Vol. 71, No. 6, September 2017, pp. 311∼318 Review Articles

Graphene-Based Vertical-Junction Diodes and Applications

Suk-Ho Choi*

Department of Applied Physics and Institute of Natural Sciences, College of Applied Science, Kyung Hee University, Yongin 17104, Korea

(Received 9 June 2017)

In the last decade, graphene has received extreme attention as an intriguing building block for electronic and photonic device applications. This paper provides an overview of recent progress in the study of vertical-junction diodes based on graphene and its hybrid systems by combination of graphene and other materials. The review is especially focused on tunnelling and Schottky diodes produced by chemical doping of graphene or combination of graphene with various semiconducting/insulating materials such as hexagonal boron nitrides, Si-quantum-dots-embedded SiO_2 multilayers, Si wafers, compound semiconductors, Si nanowires, and porous Si. The uniqueness of graphene enables the application of these convergence structures in high-efficient devices including photodetectors, solar cells, resonant tunnelling diodes, and molecular/DNA sensors.

PACS numbers: 72.80.Vp, 73.40.-c, 73.22.Pr, 61.48.Gh, 61.72.U-
Keywords: Graphene, Vertical-junction, Tunneling diodes, Schottky diodes, Photodetectors, Solar cells, Sensors, Resonant tunneling
DOI: 10.3938/jkps.71.311

I. INTRODUCTION

Graphene, two-dimensional atomic crystal, certainly has the potential for replacing some of the materials used in current technologies, in view of its extreme excellence in mechanical strength/flexibility, elasticity/transparency, electrical/thermal conductivity, and many others [1–3]. Despite the absence of a bandgap in graphene, its electronic and photonic applications are being intensively developed by engineering the characteristics with various techniques, such as bias doping for homojunctions [4–7], incorporation of foreign atoms for electronic-structure engineering [8–11], nanoscale cutting into nanoribbons/quantum dots [12–16], active construction of heterojunctions with the available materials [17–19], and so on. Electric-field doping [4, 5] and chemical doping [6, 7] have been employed to form lateral-type graphene p-n homojunctions, which cannot fundamentally show rectifying behaviors due to the Klein-tunneling effect [20], not promising for their device applications. It has been recently reported that vertical graphene heterostructures with semiconducting or insulating barriers without real doping show interesting behaviors of high on/off ratio [17], electroluminescence [18], and negative resistance [19]. However, all these studies are based on field effect transistor (FET) structures containing mechanically-exfoliated graphene, not suitable for practical large-scale device applications. As another type of vertical graphene heterojunction, there have been several reports on chemical-vapor-deposition (CVD)-grown graphene/bulk-Si heterostructures, especially for photovoltaic applications [21, 22], where the graphene film does not only enhance light transmission into Si substrate but also develops the built-in electric field by forming an interface Schottky junction with Si [22, 23]. This review focuses on the recent studies of the graphene-based vertical-junction diodes and applications. For realizing the rectifying behaviors of the vertical junctions, several kinds of doping materials and low-dimensional nanomaterials are employed. These vertical-junction diodes show remarkable sensing characteristics, promising for their applications in optical, molecular, and bio sensors. In the second section, the main characteristics of tunneling-type vertical-junction diodes fabricated by employing pristine/doped graphene layers, boron nitrides, Si quantum dots (SQDs), and their photodetectors (PDs) or resonant tunneling diodes (RTDs) applications are discussed. In the third section, the Schottky-type vertical-junction diodes made of graphene/conventional and low-dimensional semiconductors and their PDs, solar cells, or molecular-/biosensors applications are discussed. The main issues and significance of the graphene-based vertical-junction diodes are summarized in the final section.

*E-mail: sukho@khu.ac.kr

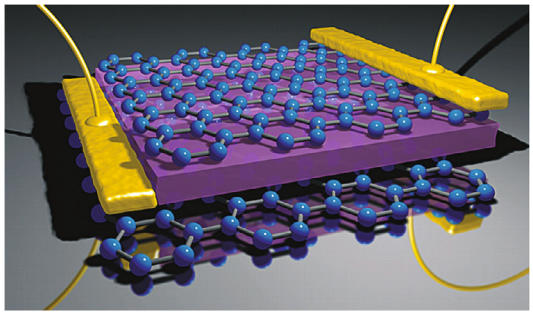

Fig. 1. (Color online) Schematic diagram of a typical graphene/hBN/graphene heterostructure tunneling diode. (Ref. [25])

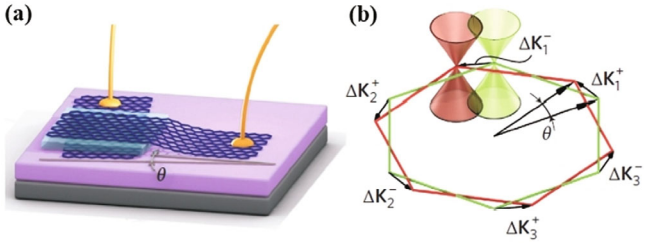

Fig. 2. (Color online) (a) Device schematics with an angle θ between two graphene layers separated by a hBN tunnel barrier. The heterostructure is placed on a SiO_x/Si substrate, which serves as a gate. Both graphene layers are independently contacted to Cr/Au electrodes. (b) A rotation by θ of the two graphene layers in real space corresponds to the momentum shift $\Delta K_I^{\pm}$ between two Dirac points. (Ref. [28])

II. TUNNELLING DIODES

1. GRAPHENE/BORON NITRIDES

Heterojunctions made of a hexagonal boron nitride (hBN) layer sandwiched between two metallic graphene layers have shown interesting rectifying behaviors [24,25] because the charge carriers should tunnel through the insulating hBN barrier for their transport. The tunneling current depends exponentially on the number of hBN layers, down to a single layer. Figure 1 shows a schematic for a typical structure of the graphene/hBN tunneling diode. Similar electron tunneling has been also observed through hBN layers on gold-coated mica by using conductive atomic force microscopy [24]. The barrier height for tunneling and dielectric breakdown strength of hBN was estimated to be 3.03 ± 0.3 eV and 7.94 MV/cm, respectively. These results demonstrate that atomically-flat and ultra-thin hBN is very useful as a defect-free dielectric in tunneling-junction diodes. In a type of FET containing the heterojunctions, the tunneling between the two graphene electrodes can be controlled by utilizing a third (gate) electrode [26,27].

As another approach for the tunneling behaviors, two graphene electrodes separated by a hBN layer were misaligned by several degrees [28], which leads to a rotation of the two graphene Brillouin zones in momentum space, as shown in Fig. 2. In this twist-controlled RTDs, resonance peaks are observed in the current-voltage characteristics, resulting in a large negative differential resistance (NDR), which induces a tunable oscillating current, useful for their applications in high-frequency devices. The bias position of the resonant tunneling can be shifted by the twisted orientation between the two graphene layers and by the external magnetic field.

2. DOPED p-/n-GRAPHENE LAYERS

Graphene p-n junctions are known not to show rectifying behaviors due to the Klein-tunneling effect [20], as demonstrated in the lateral-type ones fabricated by several techniques such as electric-field gating [4,5] and chemical doping [6,7]. In contrast, vertical-type graphene p-n junctions have shown tunnelling-diode behaviors with an on/off ratio of $\sim 10^3$ under bias voltages below ±10 V, as shown in Figs. 3(a) and (b) [29]. The interlayer formed by high-concentration doping of benzyl viologen (BV) as an n-type dopant is highly resistive and strongly corrugated, as characterized by structural/electrical/optical analysis tools, and acts as a tunnelling barrier between the metallic p and n graphene layers. The local minimum in the current-voltage (I-V) curves, typical of a tunnelling diode, is observed experimentally as well as theoretically at room temperature, as shown in Figs. 3(b) and (c), and is more clarified at lower temperatures [9,29]. The tunneling current decreases as the forward bias increases because the joint density of states has a minimum, as shown in Fig. 3(d). However, such phenomenon does not happen for reverse bias because the joint density of states increases as the bias increases, as shown in Fig. 3(e).

The graphene p-n vertical-junction diodes have also shown excellent PD characteristics of $10^{11} \sim 10^{12}$ cm $Hz^{1/2}W^{-1}$ detectivity, $0.4 \sim 1.0$ AW^{-1} responsivity, and $100 \sim 150\%$ quantum efficiency in the broad spectral range from ultraviolet to near-infrared [9]. These high-performance PD parameters are comparable to or even better than those of commercially-available Si or compound-semiconductor PDs, and can be understood by the large photocurrent gain, as proved from the fast-decay curves of photocurrent, and the carrier multiplication arising from impact ionization in graphene. The graphene p-n tunnelling diodes are distinguished from the graphene/hBN/graphene heterojunctions [24,25], as explained above, in that the gating, which controls the tunnelling barrier in the latter, is replaced by the real doping of graphene layers in the former, thereby reducing the number of terminals in the device from three to two. Similar graphene p-n tunnelling diodes have been reported by employing hBN as a tunnelling barrier [30].

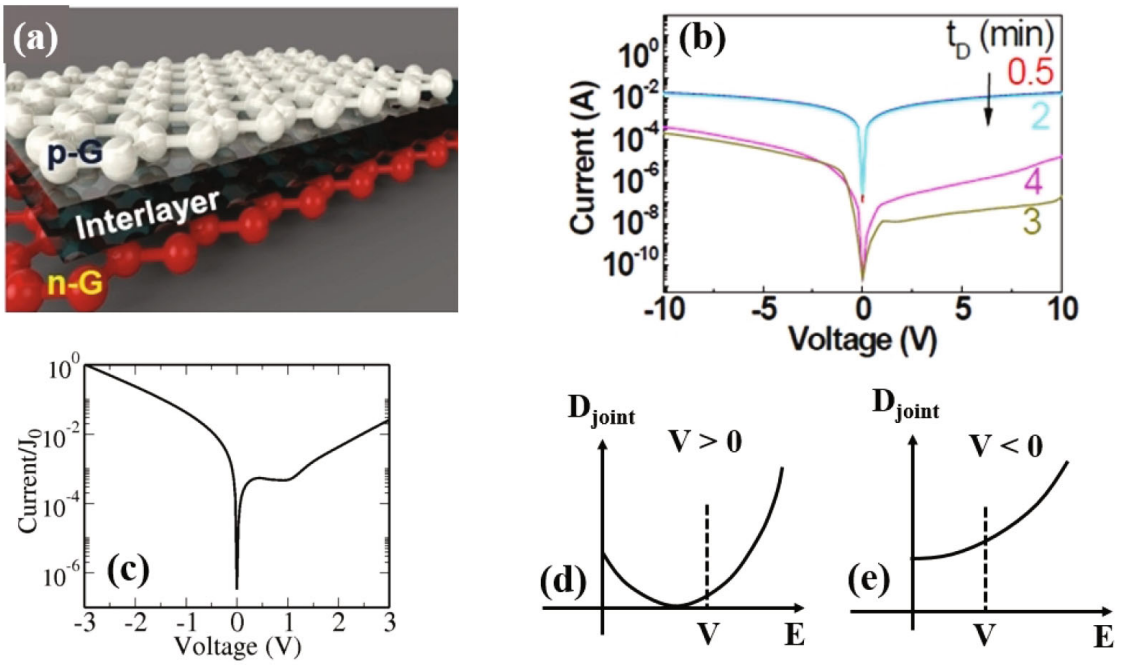

Fig. 3. (Color online) (a) Schematic of a typical graphene p-n vertical-junction tunneling diode. (b) I-V characteristics of the graphene p-n tunneling diodes. The doping time (meaning the doping concentration) for the BV exposure is 0.5, 1, 2, 3, and 4 min while the doping time for the $AuCl_3$ exposure is fixed at 5 min. (c) Theoretical I-V curve of a typical graphene p-n tunnelling diode. Joint density of states of a typical graphene p-n tunnelling diode as a function of voltage (d) under forward bias and (e) under reverse bias. (Refs. [9] and [29])

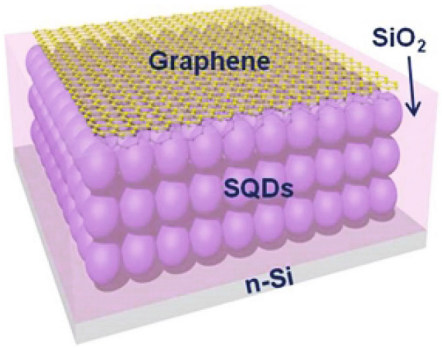

Fig. 4. (Color online) Schematic of a typical graphene/SQDs:SiO_2 MLs tunneling diode. (Ref. [38])

3. GRAPHENE/Si QUANTUM DOTS

Si is a principal material in semiconductor industries, but is of limited use in its optoelectronic device applications due to its small- and indirect- bandgap nature. To overcome this drawback, a lot of efforts have been made to employ SQDs in optoelectronic devices based on quantum confinement effect (QCE) [31, 32]. Photonic devices made of SQDs [33–37] have been intensively studied based on a structure of metal/SQDs-embedded SiO_2 (SQDs:SiO_2) single layer or multilayers (MLs)/Si wafer/metal, but their device performances are still far below commercial standards. Recently, by employing graphene as a transparent electrode, as shown in Fig. 4, the photoresponse of SQDs has been remarkably enhanced in the near-ultraviolet range compared to commercially-available bulk-Si PDs [38], as shown in Fig. 5. The observed unique PD characteristics are dominated by the tunneling of charge carriers across the SQDs:SiO_2 MLs, based on the band profiles depending on bias, size, and doping, resulting in novel dark-/photocurrent behaviors.

A phenomenon of light-induced NDR (LNDR), the basic principle of RTDs, has been observed in graphene/SQDs:SiO_2 MLs tunneling diodes [39], which is a first finding in graphene-based devices. The LNDR does not depend only on SQD size but also on temperature (T), as shown in Figs. 6(a) and (b), and its T dependence is strongly correlated with the T-dependent behaviors of the photocurrent decays. At higher light power, the photocurrent-voltage curves are more structured with peak-to-valley ratios over 2 even at room temperature, as shown in Fig. 6(c). The physical processes of the LNDR are well explained by resonant and non-resonant (or phonon-assisted) tunnelling of charge carriers across the graphene/SQDs:SiO_2 MLs.

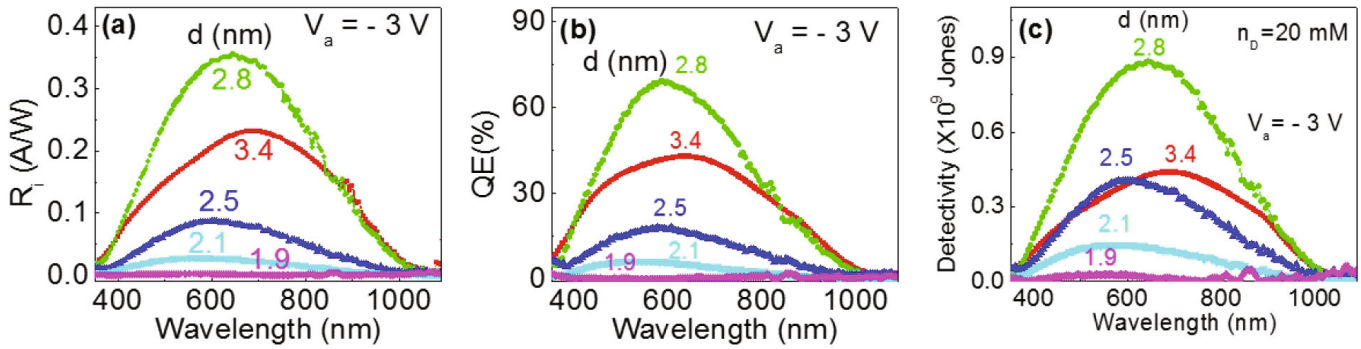

Fig. 5. (Color online) Size-dependent (a) spectral responsivity/(b) quantum efficiency/(c) detectivity for a typical graphene/SQDs:SiO_2 MLs tunnelling-diode-type photodetector at a fixed voltage of −3 V. The graphene layer was doped at an $AuCl_3$ concentration of 20 mM. (Ref. [38])

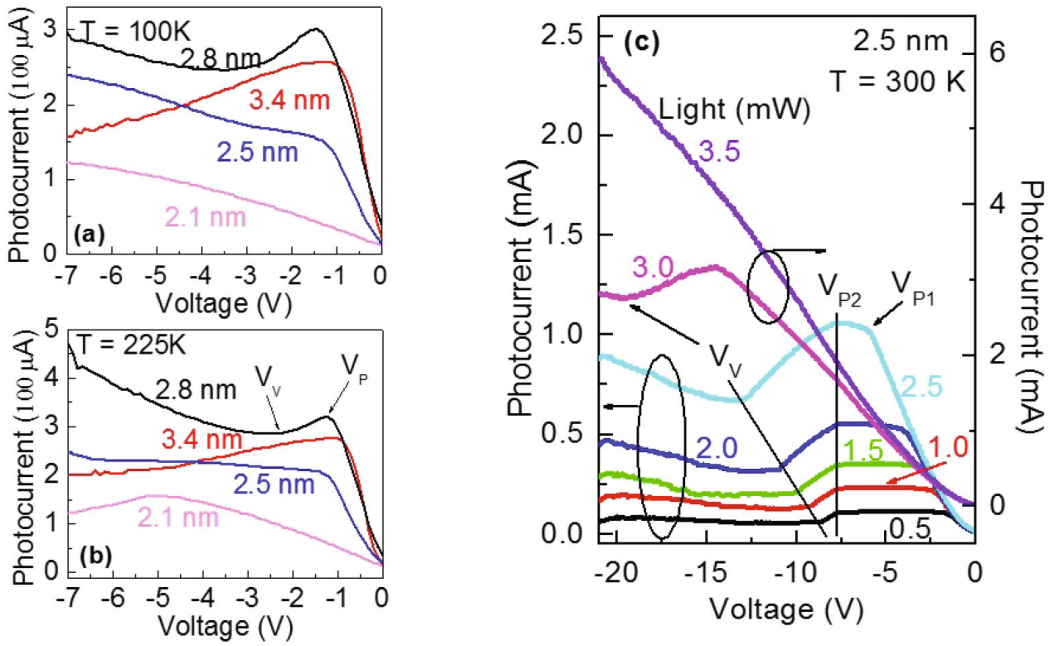

Fig. 6. (Color online) Size-dependent photo I-V curves of graphene/SQDs:SiO_2 MLs diodes at temperatures = (a) 100 K and (b) 225 K under reverse bias. The illumination was done with a light power density of 1 mW at a wavelength of 532 nm. The peak voltage V_P and the valley voltage V_V are indicated. (c) Evolution of photo I-V curves of graphene/SQDs:SiO_2 MLs diodes at room temperature for a SQD size of 2.5 nm under various light power intensities from 0.5 to 3.5 mW. The 1st peak voltage V_{P1}, 2nd peak voltage V_{P2}, and V_V are indicated. (Ref. [39])

III. SCHOTTKY DIODES

The metal/semiconductor junction, *i.e.*, the Schottky junction, is of great importance as a basic device structure in the semiconductor industries. Therefore, the graphene/semiconductor junction is highly attractive as a building block for graphene-based electronic and optical devices. The studies on the graphene/semiconductor junction, despite its importance, are currently at their early stage [40], and should be therefore done thoroughly to understand the physics and the potential applications of this device. The low density of states close to the Dirac point of graphene makes its Fermi level extremely sensitive to the number of carriers transported through the junction, which can be controlled by doping of graphene and/or semiconductor. The location of the Fermi level strongly affects the barrier height of the Schottky diode, a major factor that determines the current-voltage characteristics. In other words, the current of the graphene/semiconductor junction is tunable in various ways, useful for the practical applications. In the last several years, a few groups have demonstrated that graphene can well form junctions not only with elemental semiconductors [41–45] but also with compound semiconductors [46–51], thereby showing rectifying characteristics as excellent Schottky diodes. This is

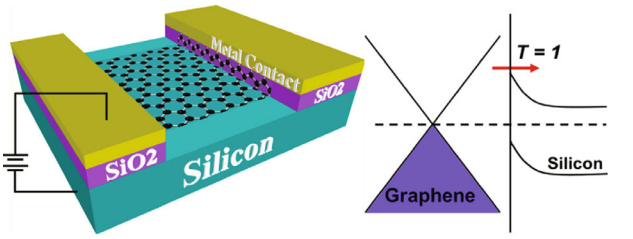

Fig. 7. (Color online) Schematic and band diagram of a typical graphene/n-Si Schottky diode. (Ref. [43])

very promising for graphene/semiconductor junction as a good platform for the study of the transport phenomena as well as for the applications in photodetectors, solar cells, high-speed devices, chemical/biological sensors, and so on.

1. GRAPHENE/Si WAFER

The graphene/Si Schottky junctions have been formed on p- or n-type Si wafers by using exfoliated graphene flakes [41] or CVD-grown graphene sheets [42–44]. Figures 7 and 8 show schematic/band diagram of a typical graphene/Si Schottky diode and its I-V characteristics. Principal Schottky-diode parameters such as barrier height and ideality factor are varied in a wide range depending on the doping type/concentration of the Si wafer [40]. The dark and photo I-V behaviors are observed with on/off current ratios of 10 to 10^{+3} at ± 1 V [52] and of more than 10^4 at -2 V [42], respectively. Higher current densities are obtained at larger doping concentration [52] and the ideality factor is almost irrespective of the doping concentration [40]. The barrier height ranges from 0.32 to 0.89 eV for the n-Si wafers and from 0.44 to 0.74 eV for the p-Si wafers depending on the doping concentration. It has been demonstrated that the graphene/n-Si wafer junctions act as highly-efficient photodetectors and solar cells with photo-responsivities and power conversion efficiencies that approach $\sim 10^7$ A/W [53] and 7.5% [54], respectively. Chemical doping of graphene is very useful for optimizing the parameters of the graphene/Si Schottky-diode solar cells [54].

2. GRAPHENE/COMPOUND SEMICONDUCTORS

Graphene-based Schottky diodes have been also fabricated on various compound semiconductors such as GaAs, GaN, CdS, and SiC [46–51]. The n-type GaAs formed Schottky junctions with bi-layer graphene to show photodetecting/photovoltaic properties of 2.88 $\times$ 1011 $Hz^{1/2}W^{-1}$ detectivity and 5 mAW^{-1} responsivity/0.65 V open-circuit voltage, 10.03 mA/cm^2 short-circuit current, and 1.95% power-conversion efficiency,

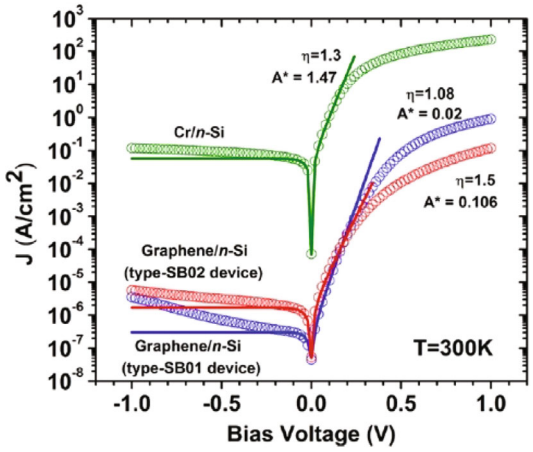

Fig. 8. (Color online) Typical current-voltage characteristics (open circles) of Cr/n-Si and graphene/n-Si and their fits (solid lines) obtained using Schottky diode model. The η is the ideality factor and the A^* is the effective Richardson constant in A/cm^2/K^2. (Ref. [43])

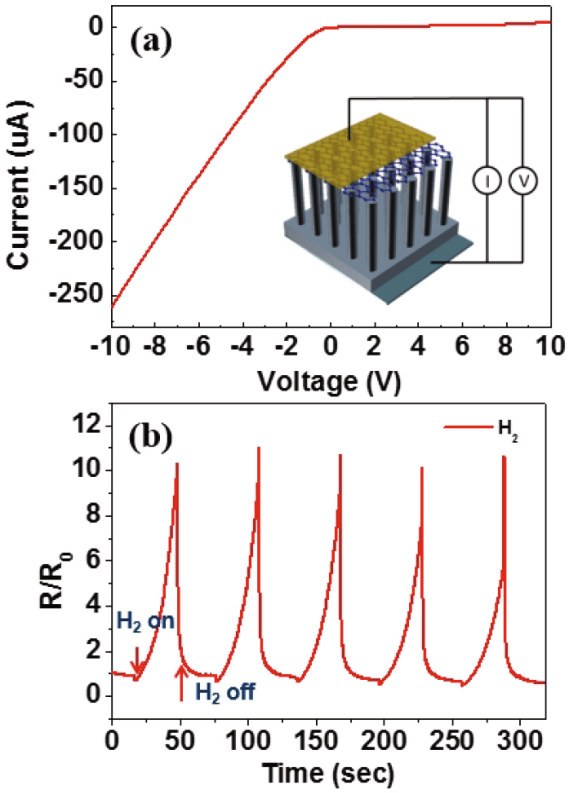

Fig. 9. (Color online) (a) I-V curve of graphene/Si-NW array heterostructure, together with a schematic illustration of the measurement configuration. (b) Normalized resistance response of graphene/Si-NW heterostructure molecular sensor under repeated exposures of H_2 gas in air at room temperature. Exposure interval of H_2 gas is 30 s. (Ref. [56])

respectively [50,51]. The barrier height of graphene/GaN diode was found to be 0.60 or 0.72 eV [48], depend-

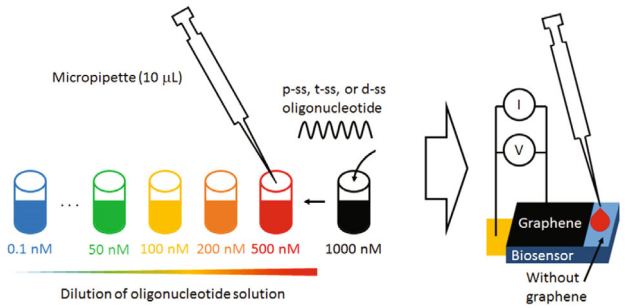

Fig. 10. (Color online) Schematic diagrams for showing the sample preparation and experimental setup for DNA sensing by using graphene/Si-NW array heterostructure Schottky diodes. (Ref. [57])

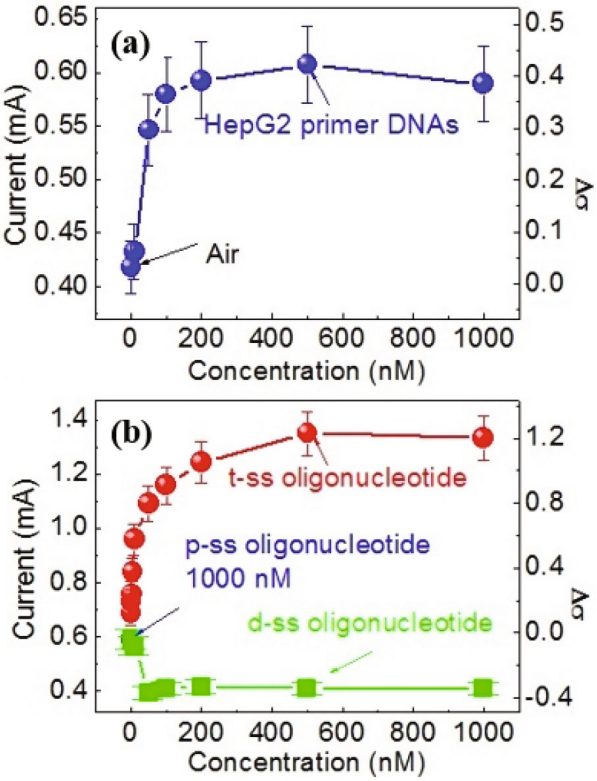

Fig. 11. (Color online) (a) Current of a graphene/Si-NWs biosensor as a function of mole fraction of *p*-ss oligonucleotide. (b) Current of a graphene/Si-NWs biosensor as a function of mole fraction of t- or d-ss oligonucleotide loaded on the surface of NWs decorated with 1000 nM *p*-ss oligonucleotide in advance. The error bars in (a) and (b) indicate 6%. (Ref. [57])

ing on the fitting model, which are by 0.3 $\sim$ 0.40 eV larger than theoretically predicted, possibly resulting from hole doping of graphene due to the interaction of graphene and Au electrode. The Schottky junctions of GaN with mechanically-foliated graphene were stably rectifying with a barrier height of $\sim$ 0.74 eV and an ideality factor of $\sim$ 2.9 up to 550 K, but above 650 K, they were non-rectifying [49]. The diodes were recovered with better rectification after cooling due to the improved interface. The graphene-based Schottky diodes were compared for principal semiconductors to extract intrinsic effects at the junctions [46,47].

3. GRAPHENE/Si NANOWIRES

Graphene has been also combined with Si nanowires (NWs) to form Schottky diodes [55], but has not shown high-quality device performance because the graphene is not well defined and the Si NWs are irregular-shaped/randomly-arranged, resulting in non-uniform contact between the graphene and NWs. In contrast, single-layer graphene and high-density vertically-aligned Si NWs [56] have been employed to form uniform graphene/Si-NWs heterostructure Schottky contact exhibiting typical Schottky-diode behaviors, as shown in Fig. 9(a). The Schottky diode acts successfully as a molecular sensor with high sensitivities of 37 and 1280% resistance changes within 3.5/0.15 and 12/0.15 s response/recovery times under O_2 and H_2 exposures, respectively, as shown in Fig. 9(b).

The graphene/Si-NWs Schottky diodes have been also employed for selective and sensitive DNA detection, as shown in Fig. 10 [57]. For this study, a twenty-seven-base-long synthetic oligonucleotide as a probe DNA, which is a fragment of human DENND2D promoter sequence, is first attached on the surface of the vertically-aligned Si NWs, and the complementary oligonucleotide as a target DNA is then combined with the probe. The current of the DNA sensor increases from 19 to 120% as the molar fraction of the target DNA varies from 0.1 to 500 nM, as shown in Fig. 11. In contrast, such biosensing does not work for a dummy DNA, *i.e.*, an oligonucleotide with incompatible or mismatched sequences, indicating good selectivity of the device. Similar sensitivity and selectivity of the biosensors are also obtained from fluorescence microscopic images and spectra of the DNAs.

4. GRAPHENE/POROUS Si

Porous silicon (PSi) is attractive as a building block for the potential applications in optoelectronic devices due to its high light absorption, high photoconductive response, high optical gain, and high ratio of surface to volume [58–61]. Graphene/PSi Schottky-junction PDs have been successfully formed by using graphene and PSi as a carrier collector and a photoactive layer, respectively, [62] as shown in Fig. 12(a). The photo-responsivity and quantum efficiency of the PDs are remarkably enhanced in the near-UV range, as shown in Fig. 12(b), resulting from the high light absorption and large bandgap of PSi. The largest gain at an etching time (t_d) = 3 s,

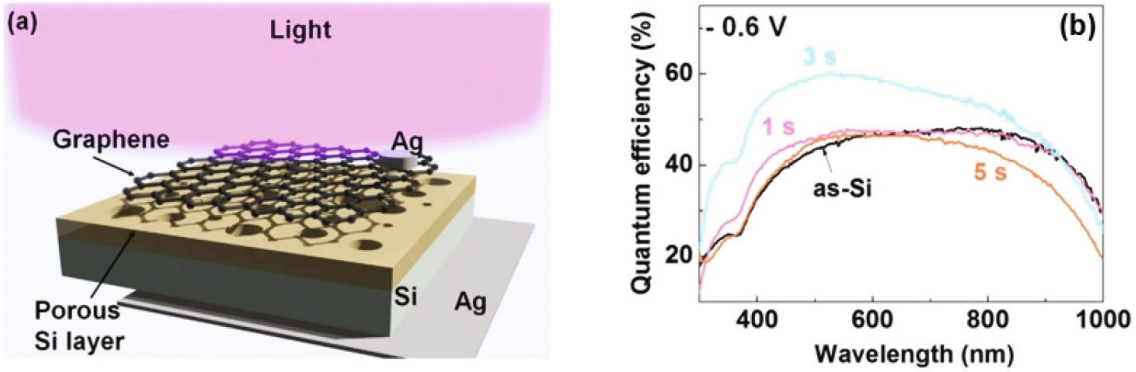

Fig. 12. (Color online) (a) A schematic diagram of graphene/PSi/n-Si photodetector with silver top and bottom electrodes under light illumination. (b) Spectral quantum efficiencies of graphene/PSi/n-Si photodetectors for various etching times of 0 (as-Si: Si wafer), 1, 3, and 5 s. (Ref. [62])

as characterized by the photocurrent decay, responsible for the maximum enhancement of the photo-responsivity and quantum efficiency in the near UV range, originating from the well-defined interface at the graphene/PSi junction at t_d = 3 s, as proved by atomic microscopy and electrostatic force microscopy. The PD characteristics are governed by the typical Schottky-type transport of charge carriers at the junction, based on the bias-dependent band profiles.

IV. SUMMARY

Tunnelling- and Schottky-type vertical-junction diodes were successfully formed by using chemical doping of graphene and combination of graphene with other semiconducting and insulating materials. The graphene vertical-junctions showed unique rectifying behaviors, resulting from actual formation of metal-insulator-metal/metal-semiconductor-metal tunnelling or metal-semiconductor Schottky diodes. The performance parameters of the PDs based on these vertical junctions are comparable to or even better than commercially-available PDs made of Si or compound semiconductor materials. In contrast, their photovoltaic characteristics are currently far below the commercial standards, but are expected to be improved by selecting optimum solar cell structures and engineering the work function of graphene. Graphene was also successfully employed in its hybrids with Si NWs for Schottky-diode-type sensors showing high molecular/bio detection efficiencies.

ACKNOWLEDGMENTS

This work was supported by Basic Science Research Program through the National Research Foundation of Korea (NRF) funded by the Ministry of Science, ICT & Future Planning (NRF-2017R1A2B3006054).

REFERENCES

[1] A. C. Ferrari *et al.*, Nanoscale **7**, 4598 (2015).
[2] K. S. Novoselov *et al.*, Nature **490**, 192 (2012).
[3] X. Zhang, B. R. S. Rajaraman, H. Liub and S. Ramakrishna, RSC Avd. **4**, 28987 (2014).
[4] B. Huard *et al.*, Phys. Rev. Lett. **98**, 236803 (2007).
[5] B. Özyilmaz *et al.*, Phys. Rev. Lett. **99**, 166804 (2007).
[6] E. C. Peters, E. J. Lee, H. M. Burghard and K. Kern, Appl. Phys. Lett. **97**, 193102 (2010).
[7] D. B. Farmer, Y-M. Lin, A. Afzali-Ardakani and P. Avouris, Appl. Phys. Lett. **94**, 213106 (2009).
[8] D. C. Elias, *et al.*, Science **323**, 610 (2009).
[9] C. O. Kim *et al.*, Nature Commun. **5**, 3249 (2014).
[10] S. Kawai1, *et al.*, Nature Commun. **6**, 8098 (2015).
[11] U. Bangert, *et al.*, Nano Lett. **13**, 4902 (2013).
[12] M. Y. Han, B. Özyilmaz, Y. Zhang and P. Kim, Phys. Rev. Lett. **98**, 206805 (2007).
[13] D. V. Kosynkin *et al.*, Nature **458**, 872 (2009).
[14] D. Pan, J. Zhang, Z. Li and M. Wu, Adv. Mater. **22**, 734 (2010).
[15] S. Kim *et al.*, ACS Nano **6**, 8203 (2012).
[16] C. O. Kim *et al.*, Scientific Reports **4**, 5603 (2014).
[17] T. Georgiou *et al.*, Science **335**, 947 (2012).
[18] F. Withers *et al.*, Nature Mater. **14**, 301 (2015).
[19] L. Britnell *et al.*, Nature Commun. **4**, 1794 (2013).
[20] A. F. Young and P. Kim, Nature Phys. **5**, 222 (2009).
[21] Y. M. Shi *et al.*, ACS Nano **4**, 2689 (2010).
[22] X. Li *et al.*, Adv. Mater. **22**, 2743 (2010).
[23] Y. Lin *et al.*, Energy Environ. Sci. **6**, 108 (2013).
[24] G. H. Lee *et al.*, Appl. Phys. Lett. **99**, 243114 (2011).
[25] L. Britnell *et al.*, Nano Lett. **12**, 1707 (2012).
[26] L. Britnell *et al.*, Science **335**, 947 (2012).
[27] L. A. Ponomarenko *et al.*, J. Appl. Phys. **113**, 136502 (2013).
[28] A. Mishchenko *et al.*, Nature Nanotech. **9**, 808 (2014).
[29] S. Kim *et al.*, ACS Nano **7**, 5168 (2013).
[30] S. H. Lee, *et al.*, Appl. Phys. Lett. **104**, 053103 (2014).

[31] L. Pavesi, L. D. Negro, C. Mazzoleni, G. FranzoÁ and F. Priolo, Nature **408**, 440 (2000).
[32] Y. Duan, J. F. Kong and W. Z. Shen, J. Raman Spectrosc. **43**, 756 (2012).
[33] A. Marconi *et al.*, Appl. Phys. Lett. **94**, 221110 (2009).
[34] A. Anopchenko *et al.*, Appl. Phys. Lett. **99**, 181108 (2011).
[35] E-C. Cho *et al.*, Nanotechnology **19**, 245201 (2008).
[36] S. H. Hong *et al.*, Appl. Phys. Lett. **97**, 072108 (2010).
[37] T. Lin *et al.*, Adv. Funct. Mater. **24**, 6016 (2014).
[38] D. H. Shin *et al.*, Advanced Materials **27**, 2614 (2015).
[39] K. W. Lee *et al.*, accepted for publication in Scientific Reports.
[40] A. D. Bartolomeo, Phys. Rep. **606**, 1 (2016).
[41] C-C. Chen, M. Aykol, C-C. Chang, A. F. J. Levi and S. B. Cronin, Nano Lett. **11**, 1863 (2011).
[42] X. An, F. Liu, Y. J. Jung and S. Kar, Nano Lett. **13**, 909 (2013).
[43] D. Sinha and J. U. Lee, Nano Lett. **14**, 4660 (2014).
[44] Y. An, A. Behnam, E. Pop and A. Ural, Appl. Phys. Lett. **102**, 013110 (2013).
[45] A. Fattah *et al.*, Small **10**, 4193 (2014).
[46] S. Tongay *et al.*, Phys. Rev. X **2**, 011002 (2012).
[47] S. Rajput *et al.*, Nature Commun. **4**, 2752 (2013).
[48] A. Kuman, R. Kashid, A. Ghosh, V. Kumar and R. Singh, ACS Appl. Mater. Interfaces **8**, 8213 (2016).
[49] S. Tongay *et al.*, Appl. Phys. Lett. **99**, 102102 (2011).
[50] W. Jie, F. Zheng and J. Hao, Appl. Phys. Lett. **103**, 233111 (2013).
[51] L-B. Luo *et al.*, J. Mater. Chem. C **3**, 4723 (2015).
[52] M. Mohammed, Z. Li, J. Cui and T-P. Chen, Nanoscale Res. Lett. **7**, 302 (2012).
[53] F. Liu and S. Kar, ACS Nano **8**, 10270 (2014).
[54] X. An, F. Liu and S. Kar, Carbon **57**, 329 (2013).
[55] H. H. Jeong *et al.*, Appl. Phys. Exp. **5**, 105103 (2012).
[56] J. Kim *et al.*, Sci. Rep. **4**, 5384 (2014).
[57] J. Kim *et al.*, accepted for publication in Scientifc Reports.
[58] X. Li and P. W. Bohn, Appl. Phys. Lett. **77**, 2572 (2000).
[59] S. K. Deb, M. Wilding, M. Somayazulu and P. F. McMillan, Nature **414**, 528 (2001).
[60] Y. Q. Qu *et al.*, Nano Lett. **9**, 4539 (2009).
[61] V. Grivickas and P. Basmaji, Thin Solid Films **235**, 234 (1993).
[62] J. Kim *et al.*, ACS Appl. Mater. Interfaces **6**, 20880 (2014).